Journal of Luminescence 202 (2018) 263–281

Contents lists available at ScienceDirect

Journal of Luminescence

journal homepage: www.elsevier.com/locate/jlumin

Photoluminescence properties of Mn^{4+}-activated oxide phosphors for use in white-LED applications: A review

Sadao Adachi

Division of Electronics and Informatics, Faculty of Science and Technology, Gunma University, Kiryu-shi, Gunma 376-8515, Japan

ARTICLE INFO

Keywords:
Phosphor
Mn^{4+}
Oxide
LED
Photoluminescence
PLE spectroscopy

ABSTRACT

The photoluminescence (PL) properties of Mn^{4+}-activated oxide phosphors are reviewed. The phosphor materials considered here are almost all the oxide phosphors ever-reported, including germinates, silicates, aluminates, perovskites, double perovskites, and so on. These oxide phosphors can be classified into three groups, namely, types A, B, and C, from their different PL spectral features. Phosphors of type A clearly reveal a zero-phonon line (ZPL) emission peak due to the $^2E_g \rightarrow {}^4A_{2g}$ transitions in the Mn^{4+} ion together with the Stokes and anti-Stokes sideband peaks; however, the type-C phosphors promise no clear identification of the ZPL emission peaks even in the PL spectra measured at cryogenic temperatures. The ZPL emission peaks in the type-B phosphors can be tentatively determined from an analysis of the PL spectra using a characteristic Poisson function. The ZPL absorption transition energies in the PL excitation spectra of the type-A, -B, and -C phosphors are determined by performing Franck–Condon analysis within the configurational-coordinate (CC) model. These transition energies and ZPL emission energies are used to obtain the crystal-field (Dq) and Racah parameters (B and C) of the Mn^{4+} ions in those Mn^{4+}-activated oxide phosphors. Temperature dependence of the PL intensity is also analyzed on the basis of the CC model and found to be in excellent agreement with the experimental data when both the optical and acoustic phonon contributions are taken into consideration in the conventional thermal quenching model.

1. Introduction

A line-shaped or a narrow-band red emission has been major requirement in solid-state lighting technologies using a white-light-emitting diode (w-LED) with an InGaN UV/blue LED chip. Thus, searching for new red-emitting phosphors containing such a red emission component is an important approach to the realization of warm w-LED devices as the next-generation light sources [1,2]. There have been mainly reported two different ions, namely, Mn^{4+} and Eu^{2+}, doped as the red-emitting activator ions in various hosts. The general performances of Mn^{4+} (Eu^{2+}) as an activator ion are peak emission at ~ 630 nm (~ 600–650 nm), excitation peak edge of ~ 450/~ 500 nm (~ 475/~ 650 nm), photoluminescence (PL) decay lifetime of a few milliseconds (a few microseconds or less), and quantum yield of ~ 80–90% (~ 80–90%). With this regard and from an economic point of view, it seems that non-rare-earth Mn^{4+} is superior than Eu^{2+}.

As a luminescence center, Mn^{4+} ion can be efficiently activated in three kinds of host materials, namely, fluorides, oxides, and oxyfluorides. In 2008, Adachi and Takahashi [3] directly synthesized K_2SiF_6:Mn^{4+} red-emitting phosphor from stain etching Si wafer in a HF solution containing a $KMnO_4$ oxidant agent. They also synthesized K_2SiF_6:Mn^{4+} by etching a crushed quartz schist or a silica glass, instead of Si wafer [4,5]. Moreover, the use of $NaMnO_4$ and $CsMnO_4$, instead of $KMnO_4$, enabled direct synthesis of Na_2SiF_6:Mn^{4+} and Cs_2SiF_6:Mn^{4+} red-emitting phosphors [6,7]. After that, various Mn^{4+}-activated fluoride phosphors have been extensively investigated for developing a new synthesis method, deep understanding red-emitting phosphor properties, and actually applying to warm w-LED devices [8,9].

The purpose of this paper is to report the PL properties of Mn^{4+}-activated "oxide" phosphors. Usually, the oxide compounds are synthesized by a high-temperature solid-state reaction method. Such oxides have excellent material properties, such as high melting point, high elastic modulus, hardness, high refractive index, and larger transparency. As a result, the oxide materials have good thermal and chemical stabilities that may provide a great advantage in the performance of highly stable w-LEDs using them as the host materials of Mn^{4+} activator ions.

There have been reported various kinds of Mn^{4+}-activated oxide hosts, including germinates, silicates, aluminates, perovskites, double perovskites, and so on. Here, we classified Mn^{4+}-activated oxide phosphors into three groups, namely, types A, B, and C, from their different PL spectral features. The zero-phonon line (ZPL) emission and

E-mail address: adachi@gunma-u.ac.jp.

https://doi.org/10.1016/j.jlumin.2018.05.053
Received 21 April 2018; Received in revised form 20 May 2018; Accepted 21 May 2018
Available online 24 May 2018

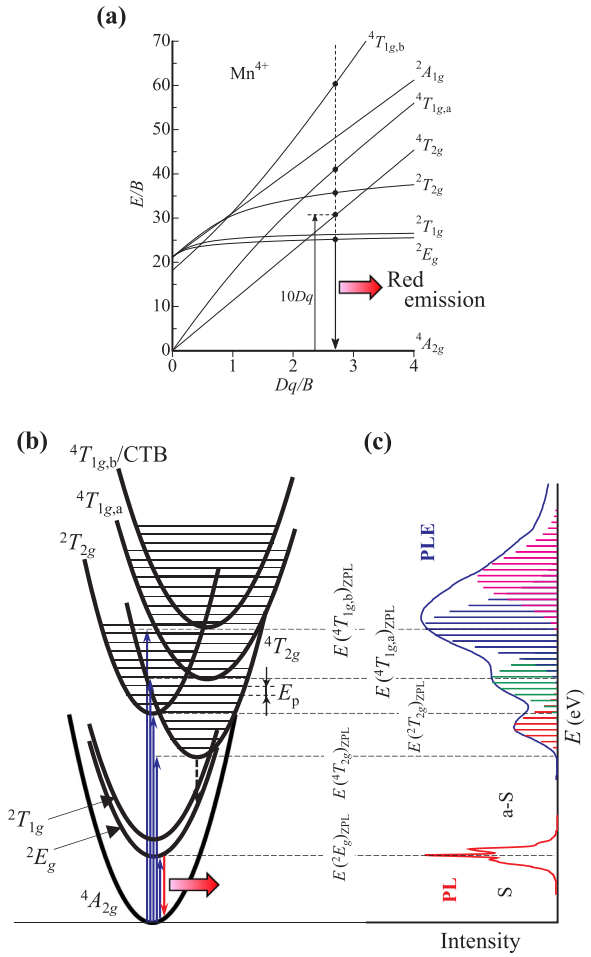

Fig. 1. (a) Tanabe–Sugano energy-level diagram for a $3d^3$ system in octahedral symmetry (Mn^{4+}). (b) CC model representing PL emission and excitation absorption transitions. (c) Schematic representation for the PL and PLE spectra of the Mn^{4+}-activated oxide phosphor. The vertical bars in the PLE spectrum [(c)] represent the theoretical model fits using Eq. (2) [Eq. (3)]. S = Stokes; a-S = anti-Stokes.

excitation energies for the Mn^{4+} ions in such oxide phosphors are determined directly from PL spectra and analyzing PL excitation (PLE) spectra by Franck–Condon analysis within the configurational-coordinate (CC) model. The ZPL emission and excitation energies are then used to obtain the crystal-field and Racah parameters of Mn^{4+} ions in these oxide hosts. A theoretical model for the temperature dependence of PL intensity over the wide temperature range from cryogenic up to ~ 500 K is presented and discussed in detail.

2. Theoretical background

2.1. Tanabe–Sugano energy-level diagram and Mn^{4+} energy levels

The influence of the crystal field on the energy levels of the $3d^n$ system can be interpreted by the Tanabe–Sugano energy-level diagram [10,11]. The optical properties of some transition metal ions with $3d^3$ ($n = 3$) configuration, including Mn^{4+}, Cr^{3+}, and V^{2+} ions, have been investigated in terms of the Tanabe–Sugano energy-level diagram with considerable success. We show in Fig. 1(a) the Tanabe–Sugano diagram for the $3d^3$ configuration of Mn^{4+} ion in an oxide host. The parabolic bands in Fig. 1(b) are schematically represented on the basis of the CC model with $^4A_{2g}$ as the ground state.

Various Mn^{4+}-doped oxide phosphors show a series of relatively sharp emission peaks in the red spectral region ~ 630–730 nm. These emission peaks are caused by the $^2E_g \rightarrow {}^4A_{2g}$ transitions. At low temperatures, only the Stokes $^2E_g \rightarrow {}^4A_{2g}$ emission peaks are observed in various phosphors (see, e.g., Fig. 4 below), which are in direct constant to the PLE spectra where only the anti-Stokes absorption peaks can be definitely observed (see details in Arai and Adachi [12]). Note that the $^4A_{2g} \leftrightarrow {}^2E_g$ transitions in the Mn^{4+} ion are parity and spin forbidden, but gain intensities with the activation of lattice vibronic modes and, as a result, become observable [9,13].

In principle, the lowest parabolic energy curve of ^2E_g in Fig. 1(b) acts as states of not only the PL but also the PLE transitions. In fact, the ^2E_g-related PL and PLE peaks have been clearly observed in the Mn^{4+}-activated fluoride phosphors [12]. However, there has been reported no PLE peak due to the $^4A_{2g} \rightarrow {}^2E_g$ transitions in the Mn^{4+}-activated oxide phosphors until now.

The $^4A_{2g} \leftrightarrow {}^2T_{1g}$ absorption/emission transitions are parity and spin forbidden. Any clear $^2T_{1g}$-related absorption/emission peaks have not been observed in the PL/PLE spectra of Mn^{4+}-activated fluoride phosphors. Thus, the origin of the $^2T_{1g}$ state cannot be definitely determined, but is usually inferred to lie at ~ 0.1 eV above the ^2E_g origin [9]. Such an energy proximity relation promised that the $^4A_{2g} \rightarrow {}^2T_{1g}$ absorption peak should nearly coincide in energy with the $^4A_{2g} \leftrightarrow {}^2E_g$ absorption and emission peaks. Therefore, the usual $^2E_g \rightarrow {}^4A_{2g}$ emission intensity can be enhanced by the $^4A_{2g} \rightarrow {}^2T_{1g}$ absorption transitions followed by an electron transfer from $^2T_{1g}$ to ^2E_g in the fluoride phosphors.

The remarkably strong absorption band in the Mn^{4+}-activated fluoride phosphors comes from the spin-allowed $^4A_{2g} \rightarrow {}^4T_{2g}$ excitation transitions [Fig. 1(c)]. The subsequent higher-lying excitation transitions of $^4A_{2g} \rightarrow {}^2T_{2g}$ are parity and spin forbidden. A peak due to such parity- and spin-forbidden $^4A_{2g} \rightarrow {}^2T_{2g}$ transitions has not been clearly observed in many fluoride phosphors [9]. In the oxide phosphors, on the other hand, these parity- and spin-forbidden transitions have been sometimes observed in the spectral region between the $^4A_{2g} \rightarrow {}^4T_{2g}$ and $^4A_{2g} \rightarrow {}^4T_{1g,a}$ (^4F) transitions as a clear peak or a bump in the lower part of the $^4A_{2g} \rightarrow {}^4T_{1g,a}$ excitation band tail [Fig. 1(c)]. Note that such spin-forbidden transitions become partially allowed because of the spin–orbit coupling that is caused by the lattice vibrations (dynamic strains) and mixes the $^4A_2$, ^2E, $^2T_2$, and $^4T_2$ states [14]. Above the $^4A_{2g} \rightarrow {}^4T_{1g,a}$ transitions in energy, another excitation transitions like $^4A_{2g} \rightarrow {}^2A_{1g}$, $^4A_{2g} \rightarrow {}^2T_{2g}$, $^4A_{2g} \rightarrow {}^2T_{1g}$, and $^4A_{2g} \rightarrow {}^4T_{1g,b}$ (^4P) are expected to occur [10,11,15]. A charge-transfer band (CTB) can also be observed in this spectral region. As a result, we can observe PLE spectra at energy above the $^4A_{2g} \rightarrow {}^4T_{1g,a}$ transitions as a very broad band with containing several kinks [see Figs. 1(c) and 3 below]. In Fig. 1(b), such higher-lying excitation bands are very indistinguishable and, therefore, we simply represented these excitation bands only by $^4T_{1g,a}$ and $^4T_{1g,b}$/CTB in the following.

2.2. Spectral feature of emission and excitation absorption transitions

2.2.1. Configuration-coordinate (CC) model

The Franck–Condon analysis with the CC model can be used to explain the optical properties of solids [16]. Here, the positions of the optical absorption and emission lines in the CC model are written as [16–18]

$$h\nu_{ex} = E_{ZPL} + kh\nu_{p,ex} \quad (1a)$$

$$h\nu_{em} = E_{ZPL} - lh\nu_{p,em} \quad (1b)$$

where h is the Planck constant, $h\nu_{p,ex}$ and $h\nu_{p,em}$ are the lattice vibronic quanta for the excited and ground states, respectively, and k and l are positive integers. The experimental absorption and emission bands can be regarded as envelopes of numerous lines; each is due to a transition between one vibrational level, k, of the excited electronic state and one vibrational level, l, of the ground electronic state.

Some of the optical spectra have a vibrational oscillation structure